Catalysis Communications 87 (2016) 98–101

Contents lists available at ScienceDirect

Catalysis Communications

journal homepage: www.elsevier.com/locate/catcom

Short communication

Silica induced oxygen vacancies in supported mixed-phase TiO_2 for photocatalytic degradation of phenol under visible light irradiation

Lan Wang [a,*], Xu Wang [b], Jiao Yin [a], Yunqing Zhu [a], Chuanyi Wang [a,*]

[a] *Laboratory of Environmental Sciences and Technology, Xinjiang Technical Institute of Physics & Chemistry, Key Laboratory of Functional Materials and Devices for Special Environments, Chinese Academy of Sciences, Urumqi 830011, China*

[b] *Laboratory of Green Chemistry and Organic Synthesis, Xinjiang Technical Institute of Physics & Chemistry, Chinese Academy of Sciences, Urumqi 830011, China*

ARTICLE INFO

Article history:
Received 18 May 2016
Received in revised form 17 August 2016
Accepted 12 September 2016
Available online 12 September 2016

Keywords:
Silica nanosheets
Oxygen vacancies
Supported TiO_2
Phenol degradation
Visible light

ABSTRACT

Phenol degradation with TiO_2 has attracted a great deal of interest in recent years. However, its low efficiency under solar radiation and difficulty of recovery limit the potential use. Here we report a novel "silica support inducing oxygen vacancies" strategy to prepare visible-light-active TiO_2 with mixed-phase, which show excellent photocatalytic performance for phenol degradation under visible light. Hydroxyl and superoxide radicals were the main oxidative species responsible for the degradation of phenol. Our work demonstrates that coupling with oxygen vacancy creation and silica nanosheets (SNSs) immobilization for TiO_2 is a new approach to obtained efficient visible-light photocatalysts for practical application.

1. Introduction

Solar energy is a clean and abundant renewable energy source available. The visible light accounts for the largest proportion of the solar spectrum (~43% of total solar energy) [1]. Thus, great interests in heterogeneous photocatalysis technology have been focused on photocatalytic degradation of organic pollutants under visible light irradiation [2,3]. This is promising for energy and environmental issues. Phenolic compounds are toxic and biorecalcitrant organic pollutants that can be found mainly in industrial wastewaters from oil refining, coking plants, steel industry, pharmaceuticals industry, and so on [4,5]. Photocatalytic degradation of phenol with TiO_2 has attracted extensive attention in environmental remediation because of its low cost, nontoxicity, stability and high efficiency properties [6]. However, TiO_2 can utilize only a small fraction of solar energy (UV light, <5% of the solar energy) for such photodegradation due to its relatively wide band gap (~3.2 eV for the anatase phase) [1]. To make full utilization of solar energy, various strategies have been developed to modify the band structure of TiO_2 to shift its photoresponse from UV to visible light region for phenol degradation [7]. In particular, recent studies have revealed that defect engineering can be utilized as an effective strategy for narrowing the band gap of TiO_2 [8–10]. Oxygen vacancy, one of the most important defect in TiO_2 materials [11,12], can creates localized states in the band gap, which could extend its optical absorption to the visible region. The conventional route for the synthesis of TiO_2 with oxygen vacancies is hydrogen thermal treatment or thermal treatment under oxygen-depleted conditions or plasma treatment [10,13,14]. But most of the preparation procedures are expensive and complicated. Therefore, it is a challenge of great importance to develop novel routes to prepare visible-light-responsive TiO_2 photocatalysts.

In a visible light photocatalysis system, the main problem is the oxidation of adsorbed organic pollutants with reactive oxygen species (ROS) based on an electron-hole pair photogeneration followed by the interfacial electron transfer or energy transfer processes. Thus, it is very important to optimize the photogenerated electron/hole separation characteristic over the TiO_2 surface. Notably, mixed-phase TiO_2 could effectively reduce the photogenerated electron/hole recombination such as Degussa P25 [15]. Additionally, nanosized TiO_2 is not convenient to use and hard to recycle due its agglomeration and low specific surface area. Based on these reasons, supported mixed-phase TiO_2 photocatalysts on clay minerals or modified clay minerals are receiving increasing attention [16,17].

However, to the best of our knowledge, less attention has been paid to develop oxygen defected and supported mixed-phase TiO_2 simultaneously for phenol degradation under visible light to date. Herein, we successfully prepared silica nanosheets (SNSs)-supported mixed-phase TiO_2 with visible-light photocatalytic activity by a "silica inducing oxygen vacancies" strategy via a two-step approach, including hydrothermal method followed by post-annealing based on our previous works [17,18]. The prepared TiO_2 possessed small crystallite size, large specific surface area and high crystallinity, and showed excellent

---

* Corresponding authors.
E-mail address: wanglan@ms.xjb.ac.cn (L. Wang).

http://dx.doi.org/10.1016/j.catcom.2016.09.011
1566-7367/

photocatalytic performance for the degradation of phenol under visible light irradiation. The ROS generated in the system were examined.

2. Results and discussion

Fig. 1a shows the X-ray diffraction (XRD) patterns of the TS-500 and T-500 (pure TiO_2) samples. As shown in Fig. 1, TS-500 and T-500 show some distinct peaks, which can clearly be ascribed to a ternary phases mixed TiO_2 that consists of anatase, rutile and brookite nanocrystals (JCPDS Nos. 21-1272, 29-1360 and 21-1276, respectively). In the case of TS-500, it can be found that the TiO_2 is mainly composed of anatase and a small amount of rutile and brookite structures, and the phase contents of rutile and brookite decreased when these TiO_2 nanoparticles were immobilized on SNSs (Table S1). These differences indicate that the phase formation is also critically related to SNSs used as support of TiO_2 nanoparticles in the reaction medium. Furthermore, the crystalline size of TiO_2 in TS-500 is almost 1/2 times smaller than that of pure TiO_2, which can be attributed to a large amount of TiO_2 nuclei formed rapidly in the presence of SNSs. The results imply that SNSs not only favors the formation of the anatase structure, but also strongly retard the growth of TiO_2 crystal particle in the process of hydrothermal reaction followed by post-annealing treatment.

The optical absorption of TS-500 and the transformed Kubelka-Munk spectrum calculated from the DRS are shown in Fig. 1b. It is clear that TS-500 exhibits visible light absorption while the pure TiO_2 can absorb only UV light (Fig. S1). A possible explanation for this phenomenon is the presence of oxygen vacancies in TS-500, as evidenced by EPR study discussed in the later section. The absorption in the visible light region helps the utilization of solar light, giving rise to more photogenerated electrons and holes for subsequent photocatalytic reactions. The band gap energy of the samples can be estimated by Kubelka-Munk function [19]. Band gap energy calculated from the intercept of the tangent lines in the plots are 2.8 and 3.0 eV for TS-500 and T-500, respectively. Thus, in the case of TS-500, the decrease in the band gap compared to T-500 can be attributed to the creation of the mid-bands/band-tail states by oxygen vacancies [10,20] formed by the introduction of SNSs support. Additionally, the energy band alignment at TS-500 was examined. As shown in Fig. S2, the positive slope of the Mott-Schottky plot shows the n-type nature of TS-500. By extrapolating the $1/C^2$-V linear plot to the voltage axis intercept, the flat band potential (V_{FB}) of TS-500 was determined to be -0.46 V (vs NHE at pH 6.8) [21,22]. For n-type semiconductor, the CB potential (E_{CB}) is very close to the V_{FB}. Using the E_g of TS-500 of 2.8 eV, the VB level was then estimated to be $+2.34$ V (vs NHE). These energy levels are important parameters that decide the feasibility of charge transport of photoexcited carriers to the surface of TS-500 and subsequent interaction with O_2 and H_2O, respectively, to produce the ROS.

Fig. S3 shows the Raman spectrum for TS-500. The Raman bands at 919 and 1125 cm^{-1} can be assigned to Si-O-Ti bridging bond (Fig. S3) [23,24]. The presence of these bands indicates that the TiO_2 is bonded to the SNSs support. Fig. 1c shows the EPR spectra of TS-500 and T-500 samples. It can be seen that T-500 does not show obvious EPR signals, meaning that it is nearly free of paramagnetic species. For TS-500, a broad peak is observed at g = 2.001, which can be assigned to the single electron trapped on the oxygen vacancy states [12]. It should be noted that the oxygen vacancies formation does not accompany the formation of Ti^{3+} defects in TiO_2. This can be ascribed to the presence of a small amount of tetrahedrally coordinated Ti with more relaxed lattice symmetry constaints in the interface of Ti-O-Si, where the coordination geometry of Ti^{4+} will be need to be tuned by creating oxygen vacancies in the SNSs-TiO_2 interface [25].

Nitrogen adsorption-desorption isotherms along with the BJH pore size distributions of the samples are shown in Figs. S4 and S5. The specific surface area (S_{BET}), pore volume (V_p) and pore diameter (D_p) of the samples are listed in Table S1. As shown in Fig. S4, the isotherm of the sample is type IV (IUPAC classification) with a H1 hysteresis-loop, showing characteristic of mesoporous structures [26]. This is consistent with SEM observation that the TiO_2 nanoparticles are homogeneously distributed on the surface of SNSs, giving flat spongy-like aggregates that are covering the SNSs completely to form a thin porous TiO_2 layer (Fig. S6). Obviously, the isotherm corresponding to TS-500 differs from that of T-500 (Fig. S5), indicating that the incorporation of SNSs creates important changes in the mesoporous structures. The S_{BET} increase from 56.6 to 226.7 m^2/g, together with the pore volumes increase from 0.148 to 0.392 cm^3/g for T-500 and TS-500, respectively (Table S1). As specific surface area plays a significant role in the photocatalytic reaction due to the more active sites for the photoreaction and the adsorption of the reactant, the relatively large specific surface area of TS-500 can be favorable for an improved photocatalytic activity. The pore size distribution of TS-500 is noticeably narrow and the average D_p is about 5.7 nm, confirming good quality of the sample [27]. Whereas, T-500 exhibits a broad pore size distribution and the average D_p is about 104.2 nm, where the formation of the larger pores may be caused by the aggregation of TiO_2 particles.

The photocatalytic activity of TS-500 was evaluated by the photodegradation of phenol in aqueous solution under visible light irradiation (Fig. 2a). For comparison purposes, the direct photolysis of phenol (blank experiment) without the presence of catalyst and the degradation of phenol over T-500 were also performed; in both cases, the degree of phenol concentration change was very limited. Obviously, after visible light irradiation for 10 h, the phenol conversion was only about 10% over T-500 owing to its wide band gap, whereas it almost unchanged in the blank experiment of phenol direct photolysis, indicating that the photocatalysis of phenol was negligible under this condition. A similar phenomenon was also observed in other report [28]. In contrast, TS-500 exhibits excellent visible light driven photocatalytic performance, for which the degradation rate of phenol was 90% in 10 h. Additionally, even though phenol has limited adsorption under dark condition, it underwent efficient degradation over the TS-500 composite photocatalyst under visible light illumination (Fig. S7). Thus, the improved photocatalytic activity mainly resulted from the combined effects of the more active sites from large specific surface area and the

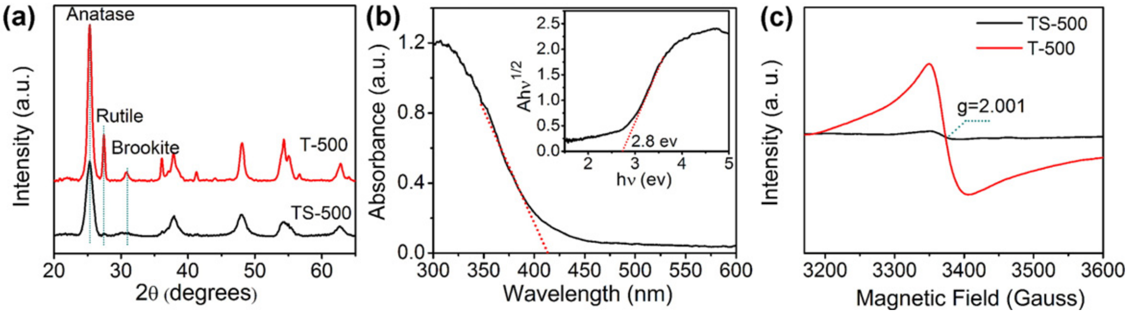

Fig. 1. (a) XRD patterns of TS-500 and T-500, (b) UV–vis diffuse reflectance spectrum of TS-500 (Inset: plot of the square root of the modified Kubelka-Munck function vs. the energy of the absorbed light), and (c) EPR spectra of TS-500 and T-500 at 273 K.